



Look, Zoom, Understand: The Robotic Eyeball for Embodied Perception

Jiashu Yang¹ Yifan Han² Yucheng Xie³ Ning Guo¹ Wenzhao Lian^{1†}

¹ School of Artificial Intelligence, Shanghai Jiao Tong University

² Institute of Automation, Chinese Academy of Sciences

³ Dalian University of Technology

jiashuyang827@gmail.com

[†]Corresponding author

Abstract

*In embodied AI perception systems, visual perception should be active: the goal is not to passively process static images, but to actively acquire more informative data within pixel and spatial budget constraints. Existing vision models and fixed RGB-D camera systems fundamentally fail to reconcile wide-area coverage with fine-grained detail acquisition, severely limiting their efficacy in open-world robotic applications. To address this issue, we propose **EyeVLA**, a robotic eyeball for active visual perception that can take proactive actions based on instructions, enabling clear observation of fine-grained target objects and detailed information across a wide spatial extent. EyeVLA discretizes action behaviors into action tokens and integrates them with vision-language models (VLMs) that possess strong open-world understanding capabilities, enabling joint modeling of vision, language, and actions within a single autoregressive sequence. By using the 2D bounding box coordinates to guide the reasoning chain and applying reinforcement learning to refine the viewpoint selection policy, we transfer the open world scene understanding capability of the VLM to a vision language action (VLA) policy using only minimal real-world data. Experiments show that EyeVLA can effectively understand scenes in real-world environments and actively acquire more accurate visual information through instruction-driven actions of rotation and zoom, thereby achieving strong environmental perception capabilities. EyeVLA introduces a novel robotic vision paradigm: under pixel and spatial budgets, it dynamically acquires highly informative visual data within given pixel and spatial budgets for environmental perception in multimodal autonomous systems.*

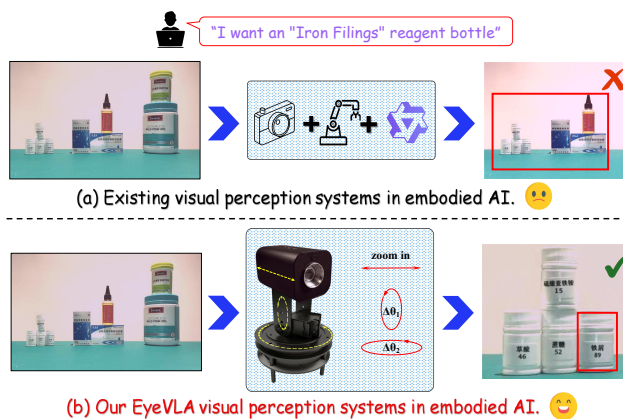


Figure 1. (a): Existing vision systems with fixed RGB-D cameras cannot handle fine-grained visual information across larger spatial extents. (b): Our EyeVLA system can perceive broader and finer-grained visual information from a fixed position by rotating its viewpoint and zooming in on the target, according to instructions.

1. Introduction

In recent years, VLMs [1, 3, 11, 15, 22] have dramatically advanced zero-shot recognition, instruction following, visual question answering, and multimodal reasoning. Modern VLMs already “understand what is in an image” to a degree that shifts the primary bottleneck in many embodied settings away from semantic inference quality towards the upstream process of acquiring the right visual evidence. Crucially, nearly all prevailing VLM paradigms still assume passively supplied, information-sufficient, static images as input; they do not decide where to look, at what scale to sense, or how to adaptively reallocate limited pixel, time, and sensing resources.

In robotics, however, perception is not a one-shot encoding problem but a sequential, resource-constrained decision process. A robot situated in a cluttered, dynamic

workspace must actively resolve uncertainty: (i) explore wide regions to localize candidate objects, then (ii) allocate as high a resolution as possible to fine-grained attributes (e.g., labels, connectors, tool tips, buttons), while (iii) strictly adhering to actuation, pixel, latency, and energy budgets. Fixed monocular/RGB-D cameras—even when coupled with powerful VLM backbones—inherently interleave information redundancy (large low-value background areas) with critical detail omissions (small, task-decisive structures). As a result, conventional VLM-based pipelines underperform on precision-sensitive tasks such as manipulation targeting, inspection, and conditional verification (e.g., “Is the small red toggle in the OFF position?”), despite excelling at global scene summarization.

This divergence exposes a structural gap: semantic reasoning has outpaced perceptual action. To bridge it, semantic intent expressed in language must be tightly coupled with viewpoint, scale, and attentional control. We thus advocate reframing language-conditioned visual perception in robots from passive inference to language-guided active acquisition—turning “answering about what is seen” into “deciding what to see next to reduce task-relevant uncertainty.”

We propose EyeVLA, a language-guided active vision framework that unifies vision, language, and embodied camera control (pan, tilt, zoom) within a single autoregressive sequence model. Concretely, we (i) discretize low-level sensorimotor adjustments into structured action tokens; (ii) interleave these with visual and textual tokens so that a pre-trained VLM can internalize viewpoint planning as part of multimodal reasoning; and (iii) impose positional (2D bounding box) feedback and reinforcement learning (RL) constraints to steer token generation toward information-efficient[27] observation policies under pixel and spatial budgets. This transforms a pre-trained passive VLM into a VLA agent with minimal additional real-device data.

In summary, our contributions are as follows:

(i) We formulate camera motion and zoom control as a discrete, tokenized decision process that is seamlessly integrated with and jointly optimized alongside multimodal reasoning, thereby transforming visual perception from passive frame consumption into a closed-loop, evidence-driven, and task-aware active acquisition paradigm;

(ii) We introduce a hierarchical discretization of pan/tilt/zoom adjustments and embed them into the VLM vocabulary, enabling unified autoregressive modeling of image, language, and action without a separate control head;

(iii) We leverage 2D region (bounding-box) signals both as structural guidance in the reasoning chain and as reward-shaping elements, yielding a RL mechanism that transfers open-world semantics to fine-grained active control;

(iv) We demonstrate a data-efficient pipeline in which, with only 500 real-world samples and pseudo-labeled expansions, EyeVLA learns actionable policies and achieves

zero-shot capability in open-world scenarios, thereby providing a practical path toward low-overhead embodiment based on existing large-scale pre-trained models.

2. Related Work

Vision Language Models. Recent advances in vision language models have enabled open-vocabulary grounding and instruction-following reasoning. Early work such as CLIP [19] aligns visual and textual representations for zero-shot image classification but lacks fine-grained spatial localization. GLIP [13] reformulates object detection as phrase grounding, enabling zero-shot localization via natural language queries. Grounding DINO [17] integrates DETR with a language encoder for high-precision, end-to-end open-vocabulary detection. In parallel, generative VLMs have advanced multimodal instruction following. LLaVA[15] and InstructBLIP[8] bridge the visual encoder and LLM via a projector, achieving alignment between vision and language. Further, Qwen-VL[2, 3] and InternVL[6] series optimized visual token compression and cross-modal alignment, achieving breakthroughs in multi-image reasoning, long-context localization, and instruction generalization, demonstrating strong general-purpose capabilities. Despite the progress in semantic and spatial understanding, existing VLMs operate on static, passively captured images, lacking control over the visual acquisition process. Our work addresses this by enabling language-guided active visual perception in dynamic environments.

Vision Language Action Models. VLA models extend VLMs to embodied control by mapping multimodal inputs directly to executable actions. Early approaches embed VLM features into policy architectures or visuomotor pipelines [20, 21], but often depend on hand-crafted structures or calibrated cameras, limiting scalability in real-world robotics. More recent methods instead fine-tune large pretrained VLMs for action generation, leveraging web-scale vision–language pretraining and general-purpose transformer backbones to align perception and control at scale [4, 10, 14, 29]. However, existing VLA models typically either attach a simple action head on top of VLM representations or directly represent actions as discrete text tokens [9, 16, 24, 26], which introduces an information bottleneck and makes it difficult to learn high-precision, fine-grained numerical control. In contrast, our approach unifies action generation and information understanding within a single autoregressive stream, preserving semantic richness while enabling more effective embodied control.

Active Perception in Robotics. Recently, there has been growing attention to active perception for robots, leading to the design of various hardware architectures [7, 18, 25]. Wang et al. [23] propose a language-driven active perception framework for navigation, where agents dynamically select camera views to resolve spatial ambiguity and ver-

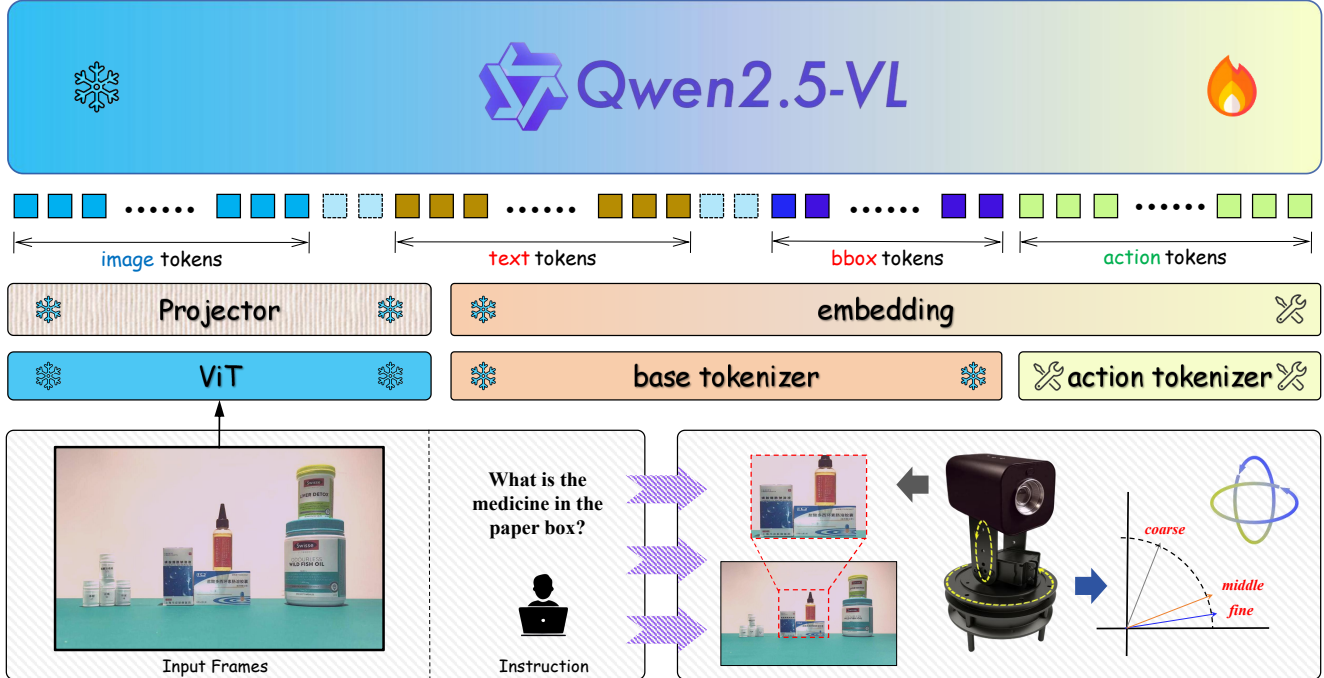


Figure 2. **Overview of EyeVLA Pipeline.** The system is built upon Qwen2.5-VL framework, integrating visual perception, language understanding, and action generation capabilities. To preserve the original semantic alignment during training, the parameters of the ViT and its projector module are kept frozen and not updated. Additionally, we introduce action tokens into the vocabulary to represent camera motions. To efficiently represent robotic actions, we further adopt a hierarchical encoding strategy to structurally model the action space.

ify object existence based on linguistic cues. LAVA [28] introduces a language-driven active vision agent that composes scene understanding through iterative visual querying — actively zooming and panning to gather fine-grained evidence for compositional reasoning. Similarly, Chen et al. [5] present a reinforcement learning approach for robotic manipulation that learns to “look before you leap”, actively adjusting viewpoint to reduce occlusion and verify affordances prior to action execution. While these methods demonstrate the value of language-guided active perception, they often rely on predefined action spaces and cascaded modules, prone to cumulated modular errors and lacking tight integration between visual/language reasoning and low-level motor control. In contrast, our system unifies language grounding, action generation, and visual feedback within a single autoregressive loop, enabling closed-loop active perception under pixel and spatial budget constraints.

3. Method

3.1. Overall approach

In this section, we elaborate on how to construct the proposed **Robotic EyeBall (REB)** system. We assembled a “robotic eyeball” capable of movement and perception in 3D space using a 2D pan-tilt mount and a zoomable camera. At the algorithm level, we adapt Qwen2.5-VL(7B) to

achieve instruction following, scene perception and understanding, and camera control (Fig. 2).

Problem Formulation. We first formally define the task studied in this paper. The input consists of two components: (a) Visual observation: an initial RGB image captured by the camera; (b) Natural language instruction: a textual command describing the desired outcome.

The goal of the system is to output a sequence of action tokens that can be decoded into camera control commands, specifically along three dimensions: Pan adjustment $\Delta\theta_1$: controls the horizontal rotation of the camera; Tilt adjustment $\Delta\theta_2$: controls the vertical rotation of the camera; Zoom adjustment Δ_{zoom} : controls the focal length.

By autoregressively predicting a sequence of action tokens, which are decoded into these three physical quantities, the system can drive the “Robotic EyeBall” to autonomously adjust its viewpoint in 3D space, aligning the resulting visual state with the semantic intent expressed in the natural language instruction, thereby achieving language-guided active visual perception.

3.2. Encoding and Decoding of actions

To enable a compact and token-efficient representation of continuous camera actions within a limited context length, we propose a hierarchical action encoding scheme that minimizes the number of tokens required to represent integer-

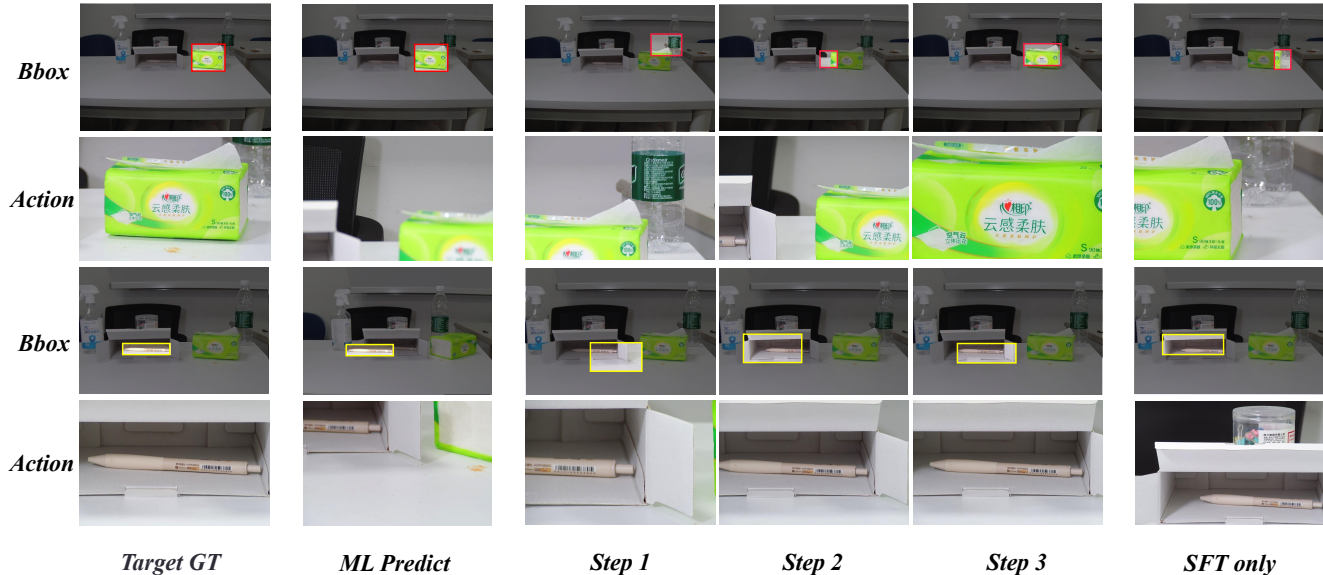


Figure 3. Inference results of models trained on synthetic data generated under different strategies and iteration counts, along with their performance comparison in real-world scenarios. The figure illustrates a scenario where the goal is to identify the brand of a pen inside a box. A conventional camera, constrained by its fixed viewpoint, cannot extend into the box via a robotic arm to capture fine details. In contrast, our EyeVLA system enables clear view of the target by dynamically adjusting the camera pose and zooming in.

valued pan and tilt angle changes ($\Delta\theta_1, \Delta\theta_2$) as well as zoom adjustments (Δ_{zoom}), while maintaining semantic coherence with the original text tokens.

Specifically, for a target angle $x \in \mathbb{Z}_{\geq 0}$, we first decompose it into decimal digits:

$$x = \sum_{\ell=0}^{L-1} x^{(\ell)} \cdot 10^\ell, \quad x^{(\ell)} \in \{0, 1, \dots, 9\}, \quad (1)$$

where ℓ denotes the digit level ($\ell = 0$: units, $\ell = 1$: tens, etc.), and L is the maximum number of digits (empirically, $L = 2$ suffices for over 98% real-world actions).

For each digit $x^{(\ell)}$, we further encode it as a non-negative integer linear combination of the basis set $D = \{5, 2, 1\}$:

$$x^{(\ell)} = \sum_{d \in D} a_d^{(\ell)} \cdot d, \quad a_d^{(\ell)} \in \mathbb{Z}_{\geq 0}, \quad (2)$$

where $a_d^{(\ell)}$ represents the coefficient for each basis element $d \in D$ in the linear combination. The encoding objective is to minimize the token count per digit:

$$\min_{\{a_d^{(\ell)}\}_{d \in D}} \sum_{d \in D} a_d^{(\ell)} \quad \text{subject to} \quad \sum_{d \in D} a_d^{(\ell)} \cdot d = x^{(\ell)}, \quad (3)$$

This formulation corresponds to the classic *Change-Making Problem* restricted to the domain $\{0, \dots, 9\}$.

Critically, the basis $D = \{5, 2, 1\}$ constitutes a *canonical coin system*. By the result of Kozen and Zaks [12], the

greedy algorithm—iteratively selecting the largest denomination not exceeding the remaining value—yields a globally optimal solution (i.e., minimal token count) for every $x^{(\ell)} \in [0, 9]$. We encode each digit place (i.e., each power of 10) using this efficient representation.

Consequently, during decoding, the original angle can be reconstructed by summing the contributions of each basis element per digit level, and the greedy strategy ensures that both encoding and decoding are computationally efficient with $O(1)$ per-digit complexity.

This design offers three key advantages: (1) theoretical optimality in token usage within each digit; (2) constant-time encoding and decoding; and (3) structural alignment with physical camera control, where higher digits correspond to coarse adjustments and lower digits to fine tuning. Empirical analysis on 500 real-world samples shows that 98.6% of actions fall within $\pm 29^\circ$, requiring at most two digit levels and achieving an average token length of 2.3—more efficient than uniform discretization (one token per degree, yielding an average length of 12.7).

3.3. Synthetic Data Generator

Initial data collection. We collect initial demonstration data by manually operating the robotic eye system to align with human-specified natural language instruction targets. Specifically, given an initial frame captured by the camera at its default pose, a human operator issues a goal-oriented natural language instruction (e.g., "What is the brand of the pen?"). The operator then manually adjusts the 2D pan-tilt

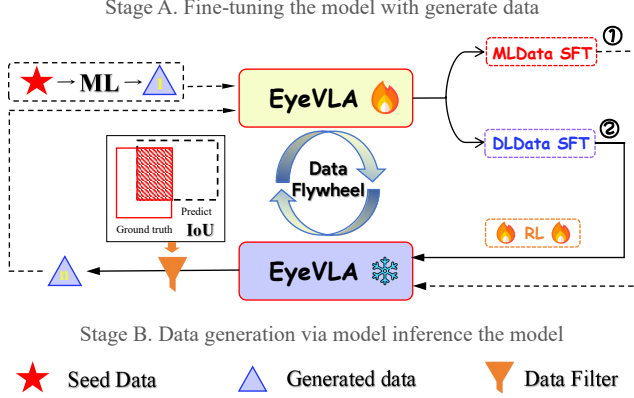


Figure 4. Flowchart of a Data Generator.

mount and zoomable camera to center and magnify the target object, recording the corresponding change signals.

$\Delta\theta_1$: horizontal pan displacement

$\Delta\theta_2$: vertical tilt displacement

Δz : zoom step change

This process yields a dataset of (instruction, initial frame, $\Delta\theta_1$, $\Delta\theta_2$, Δz , post-action frame) tuples, where the action triplet precisely realizes the intent expressed in the natural language command.

Pseudo-Label Engine. Due to the extremely high time and labor costs of manually collecting real-world data, and in order to enable the model to have strong zero-shot capability in open-world scenarios, we need to synthesize some pseudo-data that closely resembles the distribution of the original data. After task analysis, we plan to use existing grounding data (including images, references, and annotated bbox for the referred objects) for data synthesis.

Specifically, we first normalized the center coordinates of the bbox from the initial image into the range (-1, 1): the x-coordinate was normalized to model the horizontal (yaw) angle relationship, and the y-coordinate was normalized to model the pitch angle relationship. For zoom modeling, we used the ratio of the bbox area relative to the total image area before and after the zoom operation. Formally, let $w_1 = \frac{s_1}{s}$ denote the ratio of the bbox area s_1 to the total image area s in the first (pre-zoom) image, and $w_2 = \frac{s_2}{s}$ denote the corresponding ratio in the second (post-zoom) image. We then modeled zoom using the ratio w_1/w_2 .

From the Grounding dataset, we selected the 50,000 samples with the smallest target area ratios. Using the bbox descriptions in this subset, we constructed textual prompts and applied the weights learned by the Random Forest model to generate pseudo-labels. Since our simulation objective is to place the target object as large and centered as possible within the image, we performed isotropic cropping to maximize the bbox area. The cropped image

served as the adjusted ground truth, based on which we re-computed the bbox area ratio to obtain an updated w_2 , and subsequently generated the pseudo-labeled zoom value.

Finally, based on the hierarchical action token vocabulary, we use a greedy algorithm to encode the positive and negative yaw angles, pitch angles, and zoom values into discrete combinations of action tokens.

In the first alignment stage, we chose Qwen2.5-VL-7B-Instruct as the base model and trained it on the synthetically generated samples to learn the representation of action tokens. Building upon this preliminarily aligned model, we further refined the alignment using reinforcement learning on real-world robot-collected data.

In the second alignment stage, we used the trained model to infer action tokens on the same set of synthetic samples based on their prompts. We then filtered the samples based on a threshold of IoU greater than 0.7 between the predicted and ground truth bounding boxes. From these high-quality predictions, we extracted the corresponding action tokens and replaced the predicted bounding boxes with the ground-truth bounding boxes to construct a refined pseudo-label dataset. We performed SFT on this cleaned dataset, followed by further refinement through reinforcement learning on real-world robot-collected data.

In the third stage, we repeated the process from the second stage, but raised the filtering threshold to an IoU of 0.95 to further improve the quality of the pseudo-labels.

3.4. Two-Stage Training Strategy

Our training procedure consists of two stages: the SFT stage aims to inject action understanding and generation capabilities while preserving the alignment between vision and language; the RL stage focuses on guiding the model to learn generalization in real-world scenarios.

Stage 1: Supervised Alignment with Pseudo Labels We first perform supervised fine-tuning on the vocabulary-extended VLA model using the generated pseudo-labeled samples. The primary goal of this stage is to achieve low-cost and efficient alignment between the model’s output space and the physically meaningful action semantics, enabling the model to establish an initial association among vision, language, and action.

To preserve the visual representation capabilities and multimodal alignment acquired during pre-training, we freeze the parameters of both the Vision Transformer (ViT) encoder and the vision-language projector throughout the training process. Only the language model backbone and the newly introduced action token embeddings are updated. This approach ensures that the model retains its original prior semantics while learning the new action token representations, effectively preventing catastrophic forgetting.

Table 1. The table presents the MAE and completion rate (CR) of three actions under different methods and training stages: θ_1 and θ_2 denote rotational errors (in degrees, $^\circ$), and Zoom represents the error in zoom-in magnitude (approximately 90 corresponds to $1\times$ zoom). Lower values indicate better performance. "ML" refers to the machine learning baseline; "SFT1" and "SFT2" denote the supervised fine-tuning results at the second and third stages, respectively; "SFT(Y)" indicates that IoU-based sample selection was used, while "SFT(N)" denotes its absence; "RL2" and "RL3" correspond to RL training conducted after SFT2 and SFT3, respectively.

Metric	ML	SFT1	SFT2 (Y)	SFT2 (N)	SFT3 (Y)	SFT3 (N)	RL2	RL3
θ_1	6.44 $^\circ$	6.39 $^\circ$	3.97 $^\circ$	4.91 $^\circ$	2.94 $^\circ$	3.99 $^\circ$	3.26 $^\circ$	2.04 $^\circ$
θ_2	3.25 $^\circ$	3.09 $^\circ$	2.38 $^\circ$	4.87 $^\circ$	1.93 $^\circ$	3.62 $^\circ$	2.16 $^\circ$	1.68 $^\circ$
Zoom	137.60	118.18	90.68	130.37	68.22	99.72	71.33	65.37
CR	36%	36%	72%	56%	92%	84%	80%	96%

Stage 2: Policy Refinement via Reinforcement Learning

After completing the initial alignment, considering factors such as device errors and the inability of the target to occupy all pixels in the scene, the variations in rotation angles and zoom values are not fixed. We use Reinforcement Learning (RL) to optimize the policy to correct potential biases in the pseudo-labels and improve the model’s generalization ability. We apply Group Relative Policy Optimization (GRPO) to optimize the policy. This method leverages the advantages of group-normalized advantages and clipped probability ratios to stabilize the training process.

The GRPO objective is:

$$\mathcal{J}(\theta) = \frac{1}{N} \sum_{i=1}^N \left[\min(s_i(\theta), \text{clip}(s_i(\theta), 1 - \epsilon, 1 + \epsilon)) A_i - \beta D_{\text{KL}}(\pi_{\theta}(\cdot | q) \| \pi_{\text{ref}}(\cdot | q)) \right], \quad (4)$$

where π_{ref} denotes the initial VLM, ϵ defines the trust region for the importance ratio $s_i(\theta) = \frac{\pi_{\theta}(o_i|q)}{\pi_{\theta_{\text{old}}}(o_i|q)}$, β is the weight applied to the KL divergence penalty.

Through this two-phase training strategy, we achieved effective knowledge transfer from synthetic data, while utilizing real-world collected data as feedback to optimize the strategy. Ultimately, the VLA model was successfully developed, demonstrating excellent grounding, physical plausibility, and strong generalization capability.

4. Experiment

4.1. Experimental Settings

Dataset. We have developed a robotic eye system consisting of a two-axis gimbal and a zoom camera, and collected 500 real-world data samples based on this system. The dataset is divided into a training set (450 samples) and a testing set (50 samples). Given the inherent challenges of collecting real-world data and the reliance of model generalization and robustness on large-scale datasets, we pro-

pose a two-stage method. This method uses the Rexverse-2M dataset as the source of images and annotations, from which 50,000 images of smaller targets are extracted to generate synthetic data for dataset augmentation. We first select the 300 most standard data samples from the collected data (where the target is placed in the center of the field of view and maximized) and perform machine learning modeling using a random forest approach (Fig. 3).

Then, we use machine learning to generate preliminary annotations for the synthetic data. Finally, we apply reinforcement learning with a model trained on the adjusted vocabulary to the real training data, followed by re-annotation of the data to obtain the final pseudo-labeled data.

Metrics. To objectively evaluate the experimental results and the rationality of the proposed method, we perform evaluations in two dimensions: *quantitative metric evaluation* and *real-world scenario testing*.

(A) Quantitative Metrics and Results: We report the following evaluation metrics: Absolute error of predicted adjustments: $\Delta\theta_1$, $\Delta\theta_2$, and Δzoom ;

$$\text{MAE} = \frac{1}{n} \sum_{i=1}^n |y_i - \hat{y}_i| \quad (5)$$

(B) Real-World Scenario Evaluation: We evaluate and compare the models by measuring the task completion rate (Completion Rate, CR) in real-world scenarios.

Action tokens. We added 43 new action tokens to the Qwen2.5VL vocabulary and tokenizer to hierarchically represent the change values of $\Delta\theta_1$, $\Delta\theta_2$, and Zoom, and accordingly expanded the embedding dimensions. It is important to note that, since $\Delta\theta_1$ and $\Delta\theta_2$ represent angle changes in different directions, they have both positive and negative values, while the change values for Zoom only involve zooming in, so they are always positive.

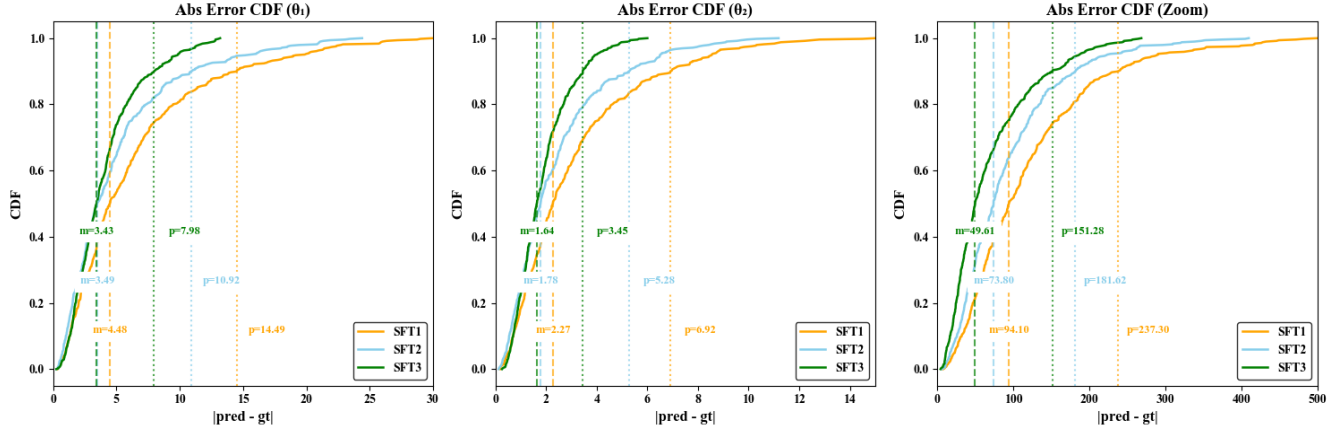


Figure 5. Comparison of Results from Three-Stage SFT

4.2. Main Results

Quantitative Comparison. We first conduct a quantitative comparison of the results from three rounds of SFT, as shown in Fig. 3. Specifically, we compute the MAE of the models after each SFT round on the test set with respect to the three variables: $\Delta\theta_1$, $\Delta\theta_2$, and Δ_{zoom} . In Table 1, we present a comparative quantitative and qualitative analysis of ablation studies, comparing the MAE scores and task success rates on the test set using different models and methods. A change of 100 in zoom value represents a doubling in the real-world scene.

To evaluate the practical applicability and effectiveness of the EyeVLA system in real-world scenarios, we conducted a comprehensive qualitative assessment across 50 real-world environments. Specifically, we selected 50 diverse real-world scenes within a controlled laboratory setting and evaluated the task completion rates of models trained using different methods. Additionally, we included a baseline machine learning approach for comparison (note: this baseline method uses real bounding boxes as one of its input features).

In Fig. 4, we present visualizations of the bbox predictions and the camera-captured images after executing actions in two different scenes with different targets, corresponding to the following two questions: “What is the brand of the tissue box?” (requiring low-resolution information from the initial state image) and “What is the brand of the pen inside the box?” (where the box space is too small to approach by driving the camera and its actuators). Clearly, through the interactive iteration between the data and the model, the model’s performance gradually improves.

Analysis of the effectiveness of action encoding and decoding. To verify the necessity of representing actions as discrete tokens, we experimented with a naive alternative: directly using the raw continuous values of the three action dimensions and training the model via SFT. However, train-

ing failed to converge, indicating that a purely continuous action representation is incompatible with the learning dynamics of our model architecture. This failure further validates the rationale behind our design choice of encoding actions as discrete tokens.

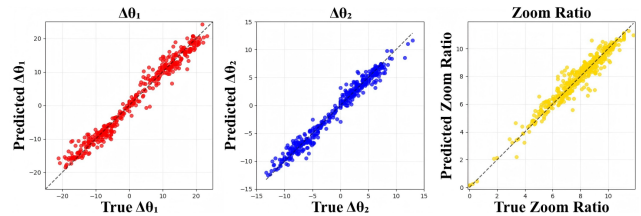


Figure 6. The fitting performance of the Random Forest

4.3. Other details

Pseudo-data Source: We randomly sampled 50,000 data pairs from the Rexverse-2M dataset, an open-world object detection dataset, and filtered for instances containing a single usable target. These were used as instruction–image pairs. Based on the learned mapping relationship, we generated the zoom and angular offset values $\Delta\theta_1$ and $\Delta\theta_2$. The relationship fitted using a Random Forest model on the data is shown in Fig. 6. The fit performs well and exhibits a strong linear correspondence, making it suitable for generating pseudo-data.

Reward Function: Our reward function is defined as a combination of the IoU of the predicted bounding box and the absolute differences between the predicted and ground-truth values for the three action outputs. The closer the predictions are to the ground truth, the higher the reward; larger deviations incur penalties.

In order to effectively guide the learning process of the model and ensure robustness by allowing a certain margin of error between the three actions and the ground truth, we

designed a linear reward mechanism based on the angle error. Specifically, when the angle error between $\Delta\theta_1$ and $\Delta\theta_2$ is less than or equal to 1 degree, the reward value increases linearly from 0 to 1; whereas when the angle error exceeds 1 degree, the model is penalized with a linear increase within the range of 0 to 1. This mechanism encourages the model to minimize the angle error, especially when high precision is required. Additionally, considering the specific requirements of real-world applications such as Zoom, when the angle error is less than or equal to the target real value and greater than or equal to the target real value minus 50 degrees, the reward value linearly changes between 0 and 1 to ensure that a reasonable reward distribution is maintained within a certain error range.

$$R = \frac{1}{4} (R_{\text{IoU}} + R_{\theta_1} + R_{\theta_2} + R_{\text{zoom}}) \quad (6)$$

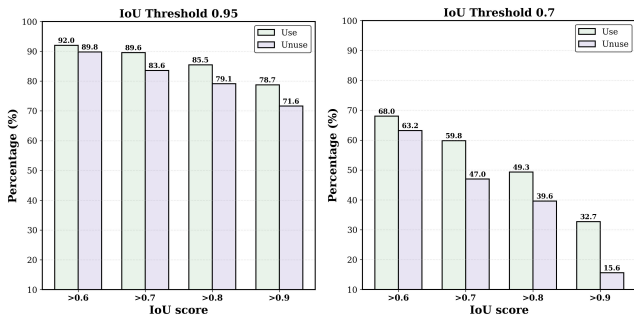


Figure 7. Comparison of IoU scores between inference results with and without the replacement strategy during training, evaluated against ground-truth annotations.

4.4. Ablation Study

IoU controlled learning. To validate the effectiveness of the IoU control strategy, we evaluated the contributions of two key components: the presence of bbox and the IoU filtering strategy, i.e., whether the bbox is present and whether IoU is filtered. Specifically, we conducted several ablation experiments: removing bbox guidance from the data and removing the IoU filtering (i.e., training using data with all IoU values). The experimental results indicate that introducing bbox guidance and the IoU filtering strategy significantly improves the model’s performance and the reliability of the data filtering strategy that uses IoU as a supervisory signal (Fig. 7).

Replacement of the bbox. To enhance the model’s ability to accurately perceive the target location, we replace the bbox annotations in the IoU-filtered training data with ground-truth bounding boxes during data iteration, thereby strengthening the supervisory signal. We compare the model performance before and after this replacement by analyzing the resulting IoU distributions and MAE under both

Table 2. Comparison of the average IoU between the two stages with and without RL.

	SFT2	RL2	SFT3	RL3
IoU	0.68	0.75	0.91	0.93

settings — use and unuse bbox replacement. The results clearly demonstrate that replacing predicted bboxes with ground-truth ones provides a more effective and positive guidance for the model.

Reinforcement Learning. To validate the effectiveness of RL, we replaced the original RL training component with SFT and evaluated the resulting model on the test set in terms of the MAE of the three action variables ($\Delta\theta_1$, $\Delta\theta_2$, and zoom) and the mean IoU of the predicted bboxes. We also assessed its generalization capability and qualitative performance in real-world scenarios. The results show that incorporating RL significantly enhances the model’s robustness; by effectively preventing the action outputs from being confined to fixed or narrow ranges, RL further improves task success rates in real-world settings.

5. Conclusion and Limitation

Conclusion. In this work, we propose a novel language-guided active vision system. This framework realizes the open-world perception and understanding specified by natural language instructions through joint decision-making between VLA and hardware actuators. It enables intelligent agents to actively acquire more informative observational data under constraints of pixel and spatial budgets, effectively addressing a key limitation in current vision systems: their passive reliance on fixed inputs and inability to adaptively gather optimal visual information in dynamic, complex environments. We have designed an efficient action encoding-decoding scheme and a reinforcement learning-based multi-round data iteration method, enabling the generation of large amounts of realistic augmented data from a small amount of real data, thereby ensuring both efficient learning and strong generalization capability. The offline and real-world test results demonstrate the effectiveness and generalization of our method. We hope that EyeVLA can serve as a practical method and a new direction for interactive active visual perception in embodied AI.

Limitation. Although this method achieves impressive performance in open-world active visual perception tasks, it is still constrained by the high computational demands of VLMs and the limitations of the camera’s hardware, which affecting its applicability in real-time scenarios. These limitations can be alleviated by using lightweight VLMs and advancements in hardware technology.

Furthermore, although we use a zoom-capable camera to perform "zoom in" operations, enabling finer-grained perception over a broader area within spatial constraints, hardware limitations still hinder the exploration of more comprehensive active perception strategies, such as "zoom out" after zooming in to capture global contextual information from other regions. Our future work may extend this system to support multi-step visual perception across multiple instruction rounds, thereby enabling more flexible and adaptive active visual perception capabilities.

References

- [1] Jean-Baptiste Alayrac, Jeff Donahue, Pauline Luc, Antoine Miech, Iain Barr, Yana Hasson, Karel Lenc, Arthur Mensch, Katherine Millican, Malcolm Reynolds, Roman Ring, Eliza Rutherford, Serkan Cabi, Tengda Han, Zhitao Gong, Sina Samangooei, Marianne Monteiro, Jacob Menick, Sebastian Borgeaud, Andy Brock, Aida Nematzadeh, Sahand Sharifzadeh, Mikolaj Binkowski, Ricardo Barreira, Oriol Vinyals, Andrew Zisserman, and Karen Simonyan. Flamingo: a visual language model for few-shot learning, 2022. [1](#)
- [2] Shuai Bai, Keqin Chen, Xuejing Liu, Jialin Wang, Wenbin Ge, Sibao Song, Kai Dang, Peng Wang, Shijie Wang, Jun Tang, Humen Zhong, Yuanzhi Zhu, Mingkun Yang, Zhaohai Li, Jianqiang Wan, Pengfei Wang, Wei Ding, Zheren Fu, Yiheng Xu, Jiabo Ye, Xi Zhang, Tianbao Xie, Zesen Cheng, Hang Zhang, Zhibo Yang, Haiyang Xu, and Junyang Lin. Qwen-vl: A versatile vision-language model for understanding, localization, text reading, and beyond, 2023. [2](#)
- [3] Shuai Bai, Keqin Chen, Xuejing Liu, Jialin Wang, Wenbin Ge, Sibao Song, Kai Dang, Peng Wang, Shijie Wang, Jun Tang, Humen Zhong, Yuanzhi Zhu, Mingkun Yang, Zhaohai Li, Jianqiang Wan, Pengfei Wang, Wei Ding, Zheren Fu, Yiheng Xu, Jiabo Ye, Xi Zhang, Tianbao Xie, Zesen Cheng, Hang Zhang, Zhibo Yang, Haiyang Xu, and Junyang Lin. Qwen2.5-vl technical report, 2025. Introduces native dynamic-resolution ViT with Window Attention for efficient high-res image and long-video processing. Achieves precise object localization via bounding boxes or points, excels in document parsing and interactive tool usage. Matches GPT-4o and Claude 3.5 Sonnet. [1](#), [2](#)
- [4] Anthony Brohan, Noah Brown, Justice Carbajal, Yevgen Chebotar, Joseph Dabis, Chelsea Finn, Keerthana Gopalakrishnan, Karol Hausman, Alex Herzog, Jasmine Hsu, Jake Kuang, Sergey Levine, Yao Lu, Linda Luu, Karina Nguyen, Xi Vincent, Pierre Sermanet, Sichun Xu, and Vincent Zhao. Rt-2: Vision-language-action models transfer web-knowledge to robot control, 2023. [2](#)
- [5] Xubo Chen, Zhiwei Jia, Yuke Zhu, and Danfei Xu. Look before you leap: Learning to actively perceive for robotic manipulation, 2024. Presents an RL approach for manipulation that learns to actively adjust viewpoint to reduce occlusion and verify affordances before acting. [3](#)
- [6] Zhaoyang Chen, Weikang Shi, Yijie Zhou, Tianyu Gao, Hao Zhang, Qiyang Yu, Jiaheng Liu, Jingwen Ye, Lizhi Cheng, Kai Chen, Yu Qiao, and Hongsheng Li. Internvl: Scaling up vision foundation models and aligning for generic visual-linguistic tasks, 2024. [2](#)
- [7] Ian Chuang, Andrew Lee, Dechen Gao, M-Mahdi Naddaf-Sh, and Iman Soltani. Active vision might be all you need: Exploring active vision in bimanual robotic manipulation. In *2025 IEEE International Conference on Robotics and Automation (ICRA)*, pages 7952–7959. IEEE, 2025. [2](#)
- [8] Wenliang Dai, Junnan Li, Dongxu Li, Anthony Meng Huat Tiong, Junqi Zhao, Weisheng Wang, Boyang Li, Pascale Fung, and Steven Hoi. Instructblip: Towards general-purpose vision-language models, 2023. [2](#)
- [9] Ankit Goyal, Hugo Hadfield, Xuning Yang, Valts Blukis, and Fabio Ramos. V1a-0: Building state-of-the-art vl-as with zero modification. *arXiv preprint arXiv:2510.13054*, 2025. [2](#)
- [10] Jiangyong Huang, Silong Yong, Xiaojian Ma, Xiongkun Linghu, Puhao Li, Yan Wang, Qing Li, Song-Chun Zhu, Baoxiong Jia, and Siyuan Huang. An embodied generalist agent in 3d world. *arXiv preprint arXiv:2311.12871*, 2023. [2](#)
- [11] A. Hurst, A. Lerer, A. P. Goucher, A. Perelman, A. Ramesh, et al. Gpt-4o system card. *arXiv preprint arXiv:2410.21276*, 2024. [1](#)
- [12] Dexter Kozen and Shmuel Zaks. Optimal bounds for the change-making problem. *Theoretical Computer Science*, 123(2):377–388, 1994. [4](#)
- [13] Liunian Harold Li, Pengchuan Zhang, Haotian Zhang, Jianwei Yang, Chunyuan Li, Yiwu Zhong, Lijuan Wang, Lu Yuan, Lei Zhang, Jenq-Neng Hwang, Kai-Wei Chang, and Jianfeng Gao. Grounded language-image pre-training, 2022. [2](#)
- [14] Xinghang Li, Minghuan Liu, Hanbo Zhang, Cunjun Yu, Jie Xu, Hongtao Wu, Chilam Cheang, Ya Jing, Weinan Zhang, Huaping Liu, et al. Vision-language foundation models as effective robot imitators. *arXiv preprint arXiv:2311.01378*, 2023. [2](#)
- [15] Haotian Liu et al. Visual instruction tuning. In *NeurIPS*, 2023. [1](#), [2](#)
- [16] Jiaming Liu, Mengzhen Liu, Zhenyu Wang, Pengju An, Xiaoli Li, Kaichen Zhou, Senqiao Yang, Renrui Zhang, Yandong Guo, and Shanghang Zhang. Robomamba: Efficient vision-language-action model for robotic reasoning and manipulation. *Advances in Neural Information Processing Systems*, 37:40085–40110, 2024. [2](#)
- [17] Shilong Liu, Zhaoyang Zeng, Tianhe Ren, Feng Li, Hao Zhang, Jie Yang, Chunyuan Li, Jianwei Yang, Hang Su, Jun Zhu, and Lei Zhang. Grounding dino 1.5: Advancing open-set object detection with hybrid experts, 2024. [2](#)
- [18] Yushan Liu, Shilong Mu, Xintao Chao, Zizhen Li, Yao Mu, Tianxing Chen, Shoujie Li, Chuqiao Lyu, Xiaoping Zhang, and Wenbo Ding. Avr: Active vision-driven robotic precision manipulation with viewpoint and focal length optimization, 2025. [2](#)
- [19] Alec Radford, Jong Wook Kim, Chris Hallacy, Aditya Ramesh, Gabriel Goh, Sandhini Agarwal, Girish Sastry, Amanda Askell, Pamela Mishkin, Jack Clark, Gretchen Krueger, and Ilya Sutskever. Learning transferable visual models from natural language supervision, 2021. [2](#)

- [20] Mohit Shridhar, Lucas Manuelli, and Dieter Fox. Cliport: What and where pathways for robotic manipulation. In *Conference on robot learning*, pages 894–906. PMLR, 2022. [2](#)
- [21] Austin Stone, Ted Xiao, Yao Lu, Keerthana Gopalakrishnan, Kuang-Huei Lee, Quan Vuong, Paul Wohlhart, Sean Kirmani, Brianna Zitkovich, Fei Xia, et al. Open-world object manipulation using pre-trained vision-language models. *arXiv preprint arXiv:2303.00905*, 2023. [2](#)
- [22] Gemini Team, Rohan Anil, Sebastian Borgeaud, Jean-Baptiste Alayrac, Jiahui Yu, Radu Soricut, Johan Schalkwyk, Andrew M Dai, Anja Hauth, Katie Millican, et al. Gemini: a family of highly capable multimodal models. *arXiv preprint arXiv:2312.11805*, 2023. [1](#)
- [23] Yunhao Wang, Zhiwei Jia, Yuke Zhu, Li Fei-Fei, and Danfei Xu. Language-driven active perception for embodied navigation, 2025. Proposes language-driven active perception for navigation, where agents select views to resolve ambiguity and verify object existence based on linguistic cues. [2](#)
- [24] Junjie Wen, Yichen Zhu, Jinming Li, Minjie Zhu, Zhibin Tang, Kun Wu, Zhiyuan Xu, Ning Liu, Ran Cheng, Chaomin Shen, et al. Tinyvla: Towards fast, data-efficient vision-language-action models for robotic manipulation. *IEEE Robotics and Automation Letters*, 2025. [2](#)
- [25] Haoyu Xiong, Xiaomeng Xu, Jimmy Wu, Yifan Hou, Jeanette Bohg, and Shuran Song. Vision in action: Learning active perception from human demonstrations. *arXiv preprint arXiv:2506.15666*, 2025. [2](#)
- [26] Yantai Yang, Yuhao Wang, Zichen Wen, Luo Zhongwei, Chang Zou, Zhipeng Zhang, Chuan Wen, and Linfeng Zhang. Efficientvla: Training-free acceleration and compression for vision-language-action models. *arXiv preprint arXiv:2506.10100*, 2025. [2](#)
- [27] Yang Yu, Zhenxing Mi, Xiao Shu, Wenbin Yang, Yueyi Zhang, and Zhiwei Xiong. EvaGaussians: Event stream assisted Gaussian splatting from blurry images. In *Proc. IEEE/CVF Int. Conf. Comput. Vision (ICCV)*, pages 24780–24790, Honolulu, HI, USA, 2025. [2](#)
- [28] Yuxiang Zhang, Yifeng Huang, Yuke Zhu, Li Fei-Fei, and Danfei Xu. Lava: Language-driven active vision agent for compositional scene understanding, 2025. Introduces LAVA, an agent that actively zooms and pans to gather visual evidence for compositional reasoning (e.g., "Is the red block under the cup?"). [3](#)
- [29] Tony Z. Zhao, Ajay Mandlekar, Danfei Xu, Josiah Wong, Ruohan Zhang, Yuqing Du, Jiaman Li, Yuke Zhu, Chelsea Finn, Animesh Garg, Fei Xia, Noah Brown, Anthony Brohan, Yevgen Chebotar, Karol Hausman, Brian Ichter, Chelsea Finn, Keerthana Gopalakrishnan, Alex Herzog, Jasmine Hsu, Jake Kuang, Yao Lu, Linda Luu, Karina Nguyen, Xi Vincent, Pierre Sermanet, Sichun Xu, and Vincent Zhao. Openvla: An open-source vision-language-action model, 2024. [2](#)